Infinite Science
Publishing

*Proceedings Article*

# Investigating the Influence of Sampling Frequency on X-Space MPI Image Reconstructions

Mark-Alexander Henn [a,b,*] · Klaus Natorf Quelhas [a,c] · Solomon I. Woods [a]

[a] National Institute of Standards and Technology (NIST), Gaithersburg, MD 20899, USA
[b] University of Maryland, College Park, MD 20742, USA
[c] Universidade Federal do Rio de Janeiro, Rio de Janeiro, Brazil
[*] Corresponding author, email: mark.henn@nist.gov

**Abstract**

In this presentation we employ a direct X-space deconvolution to estimate particle distributions from MPI data. We report on how the accuracy of those estimations changes as a function of sampling frequency and compare the findings to the MPI core operator approach found in literature.

## I. Introduction

Determining the particle distribution through image reconstruction in magnetic particle imaging (MPI) is usually done using one of two ways: by employing the system matrix [1, 2] or via the X-space [3] approach. While the system matrix approach, that makes use of the whole harmonic spectrum of the measured signal and relates it to several reference measurements, tends to be more accurate, the X-space approach tends to be more flexible by relying mostly on computational resources. But, if one wishes to determine quantitative information about the particle concentration with the X-space approach, an additional processing step of deconvolving the raw image data is required.

In this work, we focus on the X-space approach, specifically on the approach introduced in [4], where the data is transformed from time to space domain by relating the time signal to the grid of measured pixels and further processing it by calculating the MPI core operator and an additional deconvolution. This approach helps to dramatically reduce the memory and, to a lesser

degree, time requirements for the reconstruction. It also potentially introduces errors into the process, such as assumptions about the point spread function (PSF) and in determining the trace operator itself by performing a linear fit of the signal to the field free point (FFP) velocity data. One way to avoid these sources of potential errors is to use the full MPI data and perform a point by point deconvolution. The biggest drawback to this approach is the amount of computational resources required. We therefore investigate how these requirements can be reduced by decreasing the sampling frequency while still achieving an accurate reconstruction in terms of simulated data.

## II. Simulation Setup

### II.I. Signal Generation

We use the computational phantom shown in Fig.1 (a) with simulation parameters from Table 1 to generate our MPI signal. Furthermore, in order to prevent us from obtaining overoptimistic results, i.e., committing an in-

verse crime [5], we add normally distributed noise $\eta$ to our simulated signal $s(t)$. We assume a mean of zero and a standard deviation that corresponds to a percentage of the maximum of the signal, such that:

$$\eta \sim \mathcal{N}\left(0, \sigma^2\right), \ \sigma = \kappa \cdot \max[s(t)]. \tag{1}$$

We use a total of four different noise levels ranging from 1% to 10%, hence $\kappa \in \{0.01, 0.03, 0.05, 0.1\}$.

## II.II. Image Reconstruction

Once we have generated the noisy signal, we need to post-process the data in order to reconstruct the particle distribution. The base algorithm to determine the particle distribution from the raw time-signal is explained in more detail in [4] and can be broken down into three steps:

1) Bin the time-signal w.r.t. its spatial position, i.e., for each pixel collect all the data for which the corresponding FFP positions fall within that pixel's boundaries. The data set we collect consists of three parts, the measured signal itself, the FFP trajectory values, and the FFP velocities, arranged as matrices $S_i$, $X_i$, and $V_i$ for the $i$-th pixel.

2) For each of those bins (pixels) solve the system of equations:

$$S_i = A_i \cdot V_i, \tag{2}$$

to determine the matrix $A_i$ and calculate its trace $u_i = \mathrm{tr}(A_i)$.

3) Deconvolve the trace data $u = [u_1, \cdots, u_n]$, using a Toeplitz matrix $K$ that consists of the PSF at every pixel position. This leads to a regression problem:

$$K \cdot \rho = u, \tag{3}$$

from which we determine the particle distribution $\rho$. Note that the regression problem in Eq. 3 might require an additional regularization step [6].

By gridding the data in this way and fitting the signal vs. velocity data in step 2), we average and therefore lose some of the information contained in the time-signal data. See Fig. 2 where we compare the data in the vector $S_i$ (Data) vs. the product $A_i \cdot V_i$ (Fit).

However, we have dramatically reduced the size of the matrices involved, since the dimensions of $K$ after this process only depend on the number of pixels in $x$ and $y$ directions, $n_x$ and $n_y$, respectively, such that $K \in \mathbb{R}^{n_x \cdot n_y \times n_x \cdot n_y}$ (this is of course an example in 2D and for problems with differing dimensions the sizes will change accordingly).

Alternatively, we can skip the gridding, i.e., use the whole data set, evaluate the PSF at every time step, and deconvolve with a matrix $K_{\text{comp}}$ whose size depends on the number of pixels in $x$ and $y$ direction and the total
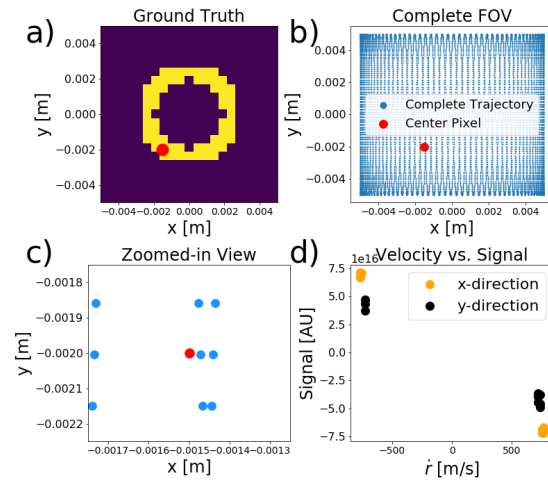


**Figure 1:** (a) Ground truth phantom used for simulations. (b) The FFP trajectory within the whole FOV. (c) Zoom of a single pixel marked in red in (a) and (b), illustrating the gridding process in which we collect all the data points (blue points) that fall within the pixel's boundaries and in (d) plot of the signal vs. velocity data. Data shown have an added noise with $\kappa = 0.05$.

number of measurements in time domain $n_t$, such that $K_{\text{comp}} \in \mathbb{R}^{n_x \cdot n_y \times 2 \cdot n_t}$. Note that the factor of 2 in the matrix's column dimension is due to the fact that we treat the signals measured at the $x$ and $y$ receive coils separately, whereas in the MPI core operator approach, we added those in step 3) by taking the trace of $A_i$.

The number of measurement data $n_t$ depends on the sampling frequency $f$ for our measurement and a reduction of that frequency consequently leads to a reduction of the size of $K_{\text{comp}}$. How a change in $f$ affects the accuracy of the reconstruction will be investigated in the next section.

**Table 1:** Simulation Parameters.

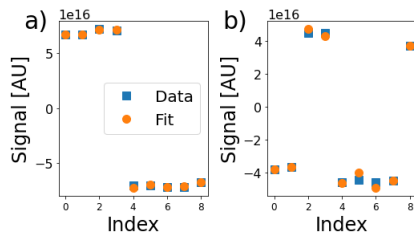| Parameter | Value |
|---|---|
| Particle Diameter | $2 \cdot 10^{-8}$ m |
| Saturation Magnetization | $4.5 \cdot 10^5$ A/m |
| Temperature | 300 K |
| Gradient in $x$-direction | 12 T/m |
| Gradient in $y$-direction | $-6$ T/m |
| Coil Sensitivity | $8.38 \cdot 10^{-4}$ T/A |
| Field of View (FOV) | $\pm 5 \cdot 10^{-3}$ m |
| Total Number of Pixels | $21 \times 21$ |
| Measurement Time | $4 \cdot 10^{-3}$ s |
| Drive Coil Frequency $x$-direction | 25.5 kHz |
| Drive Coil Frequency $y$-direction | 25.25 kHz |

**Figure 2:** Noisy data vs. fit data in step 2) of the gridding algorithm for $\kappa = 0.05$. The index refers to the different FFP positions, i.e., the blue points in Fig. 1. (a) data from the $x$ receive coil, (b) data from the $y$ receive coil. Note the deviation in the fits.
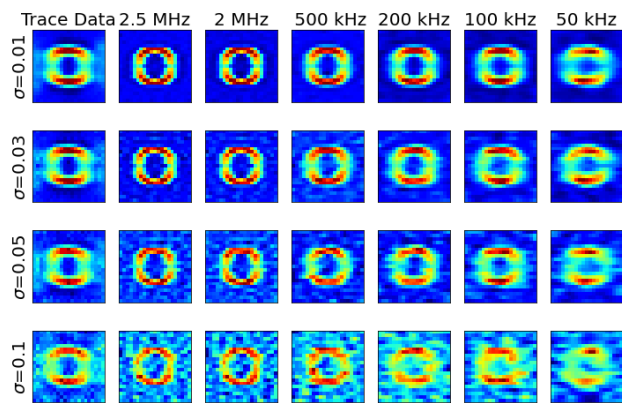


**Figure 3:** Reconstructed particle distributions for different noise levels and sampling frequencies. Left most column shows results from the trace data approach.

## III.  Results

In this section we use five different sampling frequencies between 50 kHz and 2 MHz in addition to the base sampling frequency of 2.5 MHz. For each of those frequencies we apply four different noise levels from 1% to 10% of the maximum of the time-signal. We use a gradient based Newton-CG optimization algorithm with Tikhonov regularization and manually determine the optimal regularization parameter for each fit individually.

The qualitative comparison of the reconstructed particle distributions is shown in Fig. 3. One can clearly see how the image quality decreases with decreasing sampling frequency and increasing noise level (left to right and top to bottom, respectively).

To have a quantitative understanding of the quality of the reconstructions, we also calculate the mean-square error (MSE) between the estimated particle distribution and the ground truth, shown in Fig. 4. We see that the reconstructions from the trace data remain relatively stable for the different noise levels, while the other reconstructions show a higher variance in the estimated particle distributions. However, the reconstructions from the trace data always have a worse MSE compared to the
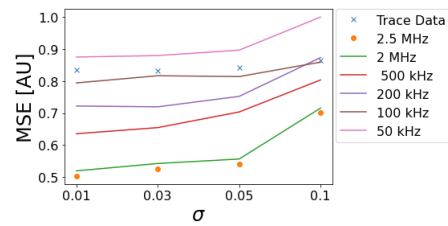


**Figure 4:** MSE between reconstructions and ground truth for different noise levels and sampling frequencies.

data with a sampling frequency above 100 kHz, and are superior to the 100 kHz data only for a noise level above 5%.

## IV.  Conclusion

In this work we have shown how a reduction of the sampling frequency impacts the accuracy of the image reconstruction for MPI if compared to the MPI trace operator approach introduced in [4]. We show that a reduction of the sampling frequency by a factor of more than twelve is possible without compromising accuracy relative to the trace operator approach.

Note that even though the total size of the matrices involved is still four times the size used in the trace operator approach, with recent developments in computation efficiency and parallelization [7] and the fact that a signal vs. velocity fit is not required, our findings imply that the direct reconstruction could be a more accurate way of MPI image reconstruction in the future.

## Acknowledgments

## Author's statement

Conflict of interest: Authors state no conflict of interest.

## References

[1]  B. Gleich and J. Weizenecker. Tomographic imaging using the non-linear response of magnetic particles. *Nature*, 435(7046):1214–1217, 2005, doi:10.1038/nature03808.

[2]  T. Knopp and T. M. Buzug, Magnetic Particle Imaging: An Introduction to Imaging Principles and Scanner Instrumentation. Berlin/Heidelberg: Springer, 2012, doi:10.1007/978-3-642-04199-0.

[3]  P. W. Goodwill, E. U. Saritas, L. R. Croft, T. N. Kim, K. M. Krishnan, D. V. Schaffer, and S. M. Conolly. X-space MPI: magnetic nanoparticles for safe medical imaging. *Advanced materials*, 24(28):3870–3877, 2012.

[4] T. März and A. Weinmann. Model-based reconstruction for magnetic particle imaging in 2D and 3D. *Inverse Problems and Imaging*, 10 (4), 2016, doi:10.3934/ipi.2016033.

[5] J. Kaipio and E. Somersalo. Statistical inverse problems: Discretization, model reduction and inverse crimes. *Journal of computational and applied mathematics*, 198(2):493–504, 2007.

[6] H. W. Engl, M. Hanke, and A. Neubauer, Regularization of inverse problems. Springer Science & Business Media, 1996, 375.

[7] K. N. Quelhas, M.-A. Henn, R. C. Farias, W. L. Tew, and S. I. Woods. Parallel MPI image reconstructions in GPU using CUDA. *International Journal on Magnetic Particle Imaging*, submitted for publication.